Mesh Adaptivity and Error Control for a Finite Element Approximation of the Elastic Wave Equation*

Wolfgang Bangerth†

Abstract

An approach to solve the elastic wave equation by adaptive finite elements is presented. The strategy for adaptivity is founded on an a posteriori residual-based error estimate, where the error is measured with respect to an arbitrary target functional, allowing to focus the simulation to the computation of a given quantity of interest. The cell-wise error indicators are computationally evaluated and used for refinement of the space-time mesh. The resulting grids are usually highly localized and tailored to the target functional. The performance of the approach is demonstrated with two examples.

1 Introduction

Adaptive methods and error estimators for the numerical solution of wave equations have not received widespread attention yet. This is despite the fact that these methods seem to be made for this class of problems due to local features of solutions, and also often localized regions of evaluation of the numerical solution; for both these localizations, it was shown in the past that they can be exploited by adaptive methods to significantly reduce the numerical effort needed to get accurate results. While these methods were usually developed for prototypic elliptic partial differential equations, the wave equation has the particular feature of a limited domain of influence, which allows for further localization.

Adaptive methods in finite element analysis are usually based on a posteriori error estimates of the numerical solution. In this presentation we present an approach which is based on a work of Eriksson and Johnson [6], which was later extended to a posteriori error estimates for the acoustic wave equation by Johnson [7]. In these works, a dual problem was introduced which is used to incorporate into the error estimates the influence of the target quantity one is interested in. However, a priori estimates were used for the solution of this dual problem in order to eliminate it again before evaluating the error estimates. This is often suboptimal in cases of localized target functionals, which is why Becker and Rannacher [5] have later extended this approach by actually computing the solution of the dual problem numerically and using it in a suitable form as weights for the error estimator; this not only allows to estimate the error in arbitrary functionals, but also to generate meshes specially tailored to the computation of this certain quantity.

The present work is an extension of a previous work using the approach outlined above for the acoustic wave equation [3].

*The author acknowledges the support by the German Research Association (DFG) through the Graduiertenkolleg and the SFB 359 at the IWR, Universität Heidelberg.

†Institute for Applied Mathematics, University of Heidelberg, Germany. Email: wolfgang.bangerth@iwr.uni-heidelberg.de

2 Finite element approximation

We start from the elastic wave equation on a space-time domain $Q_T = \Omega \times I$, $\Omega \subset \mathbb{R}^d$, $I = [0,T]$, accompanied by initial and boundary conditions:

$$\begin{aligned} \rho\partial_t^2 u_i - \partial_j c_{ijkl}\partial_k u_l = 0, \quad &\text{in } Q_T, \\ \mathbf{u}(\mathbf{x},0) = \mathbf{u}^0, \quad \partial_t\mathbf{u}(\mathbf{x},0) = \mathbf{v}^0, \quad &\text{in } \Omega, \qquad n_j c_{ijkl}\partial_j u_k = 0, \quad \text{on } \partial\Omega \times I. \end{aligned} \tag{1}$$

Summation over indices $i,j,k,l = 1,\ldots,d$ is implied where appropriate. This is transformed into weak form by first introducing a velocity variable $\mathbf{v} = \partial_t\mathbf{u}$, multiplication by a test function and integration by parts with respect to the space variables: Find $\mathbf{w} = \{\mathbf{u},\mathbf{v}\}$ from the solution space W, such that

$$a(\mathbf{w},\boldsymbol{\tau}) = (\rho\mathbf{w}^0, \boldsymbol{\tau}(0))_\Omega \qquad \forall\boldsymbol{\tau} = \{\boldsymbol{\varphi},\boldsymbol{\psi}\} \in T, \tag{2}$$

with T the test space, and the bilinear form

$$a(\mathbf{w},\boldsymbol{\tau}) = (\rho(\partial_t\mathbf{u} - \mathbf{v}), \boldsymbol{\varphi})_{Q_T} + (\rho\partial_t\mathbf{v}, \boldsymbol{\psi})_{Q_T} + (c_{ijkl}\partial_k u_l, \partial_j\psi_i)_{Q_T} + (\rho\mathbf{w}(0), \boldsymbol{\tau}(0))_\Omega . \tag{3}$$

We note that initial values have thus been integrated into the weak formulation of (1).

Based on this formulation, we seek our finite element approximation by defining suitable finite-dimensional spaces $W_h \subset W$ and $T_h \subset T$ and requiring the numerical solution to fulfill the following discrete analogue of (2): Find $\mathbf{w}_h = \{\mathbf{u}_h,\mathbf{v}_h\} \in W_h$, such that

$$a(\mathbf{w}_h,\boldsymbol{\tau}_h) = (\rho\mathbf{w}^0, \boldsymbol{\tau}_h(0))_\Omega \qquad \forall\boldsymbol{\tau}_h = \{\boldsymbol{\varphi}_h,\boldsymbol{\psi}_h\} \in T_h. \tag{4}$$

We choose W_h and T_h such that the spatial parts are standard bi- or trilinear elements (for $d = 2$ or 3) and that the time dependence allows us to recover the well known Crank-Nicolson time stepping scheme from (4). For details on function spaces and the discretization, we refer to [3].

We note that due to $T_h \subset T$, a subtraction of (2) and (4) yields the so-called Galerkin orthogonality relation for the error $\mathbf{e} = \mathbf{w} - \mathbf{w}_h$ of the finite element approximation: $a(\mathbf{e},\boldsymbol{\tau}_h) = 0$ for all $\boldsymbol{\tau}_h \in T_h$.

3 Error control

Our approach to error estimation aims at measuring the error in general functionals, not only norms. Therefore, assume the goal of a simulation is the evaluation of the functional

$$J(\mathbf{w}) = \int_{Q_T} \mathbf{j}\cdot\mathbf{w}\; dx\; dt,$$

with $\mathbf{j} = \{\mathbf{j}_u,\mathbf{j}_v\}$. We allow the kernel $\mathbf{j}$ to consist of Dirac functions and other measures, so J includes point evaluations, line integrals, and other evaluations, as long as it remains a linear functional. Extensions to nonlinear functionals have been made in [1, 4].

The aim of error control is then to estimate the difference between the exact value, $J(\mathbf{w})$, and the value computed from the numerical solution, $J(\mathbf{w}_h)$. Due to the linearity of J, this difference equals $J(\mathbf{e})$. In order to estimate this quantity, we first define a dual problem: Find $\mathbf{w}^* = \{u^*, v^*\} \in W^*$, such that

$$a^*(\mathbf{w}^*,\boldsymbol{\tau}^*) = J(\boldsymbol{\tau}^*) \qquad \forall\boldsymbol{\tau}^* = \{\boldsymbol{\varphi}^*,\boldsymbol{\psi}^*\} \in T^*, \tag{5}$$

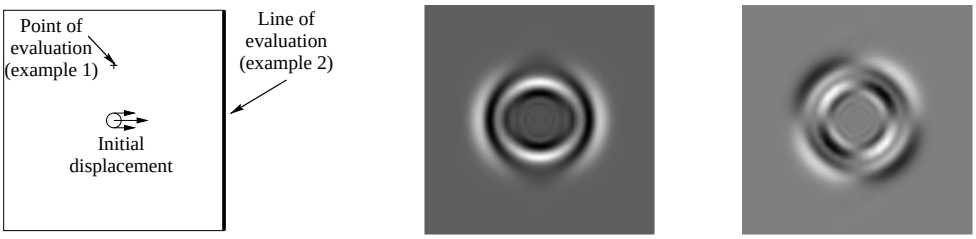

FIG. 1. *Layout for the examples, and x- and y-displacement of the numerical solution at* $t = 0.3$.

with the bilinear form $a^*(\cdot,\cdot)$ as in (3), but with the sign of the time derivative reversed and initial values replaced by final ones. Dual solution and test spaces, W^* and T^*, are chosen appropriately. This dual problem resembles a wave equation to be solved backward in time, where the integral kernel $\mathbf{j}(\mathbf{x},t)$ acts as final values, boundary conditions and sources. For example, if $\mathbf{j}_u = \delta(\mathbf{x}-\mathbf{x}_0)\delta(t-T)$, then $\mathbf{v}^*$ equals the advanced Green's function for $(\mathbf{x}_0,T)$, denoting the weight with which a space-time point contributes to the evaluation of $\mathbf{u}(\mathbf{x}_0,T)$.

The function spaces can be chosen in such a way that $\mathbf{e} \in T^*$ (see [3]). For the quantity $J(\mathbf{e})$ which we would like to estimate we then have by (5): $J(\mathbf{e}) = a^*(\mathbf{w}^*,\mathbf{e})$. Integrating by parts with respect to the time variable, we note that $a^*(\mathbf{w}^*,\mathbf{e}) = a(\mathbf{e},\mathbf{w}^*)$. Finally, using Galerkin orthogonality, we arrive at

$$J(\mathbf{e}) = a(\mathbf{e},\mathbf{w}^* - \mathbf{w}_h^*) \qquad \forall \mathbf{w}_h^* \in T_h.$$

Splitting the space-time integral in $a(\cdot,\cdot)$ into space-time cells $K \times I_n$, $K \subset \Omega$, $I_n = (t_{n-1},t_n]$, and again integrating by parts with respect to the space variables, we can eliminate the exact solution $\mathbf{w}$, and arrive at the following error representation:

$$\begin{aligned} J(\mathbf{e}) &= \sum_{n=1}^{N}\sum_{K}\eta_K^n, \\ \eta_K^n &= (\rho(\partial_t\mathbf{u}_h - \mathbf{v}_h), \mathbf{u}^* - \mathbf{u}_h^*)_{K\times I_n} + (\rho\partial_t\mathbf{v}_h, \mathbf{v}^* - \mathbf{v}_h^*)_{K\times I_n} \\ &\quad - (\partial_j c_{ijkl}\partial_k(\mathbf{u}_h)_l, (\mathbf{v}^* - \mathbf{v}_h^*)_i)_{K\times I_n} + \tfrac{1}{2}\,(n_j[c_{ijkl}\partial_k(\mathbf{u}_h)_l], (\mathbf{v}^* - \mathbf{v}_h^*)_i)_{\partial K\times I_n}, \end{aligned} \tag{6}$$

where $n_j[c_{ijkl}\partial_k(\mathbf{u}_h)_l]$ denotes the jump of the normal fluxes across the face of a cell K. Terms involving the error in the initial value between $\mathbf{w}^0$ and $\mathbf{w}_h(0)$, weighted by $\mathbf{w}^*(0) - \mathbf{w}_h^*(0)$, need to be considered here as well, but have been omitted for brevity. These error estimators do not involve the exact primal solution $\mathbf{w}$ anymore, but include the exact dual solution $\mathbf{w}^*$ instead. We evaluate the error indicators η_K^n by approximating the exact dual solution by suitable numerical approximations (see [3, 5]). The resulting values for each space-time cell are then used for error estimation as well as for refinement of the space-time triangulation.

4 Numerical examples

In this section, we will look at two examples in order to demonstrate the performance of the approach derived above. We will in both examples assume the material to be isotropic, i.e. $c_{ijkl} = \lambda\delta_{ij}\delta_{kl} + \mu(\delta_{ik}\delta_{jl} + \delta_{il}\delta_{jk})$, with Lamé's coefficients $\lambda = \mu = 1$ for simplicity. The computations were performed with a program based on the `deal.II` library

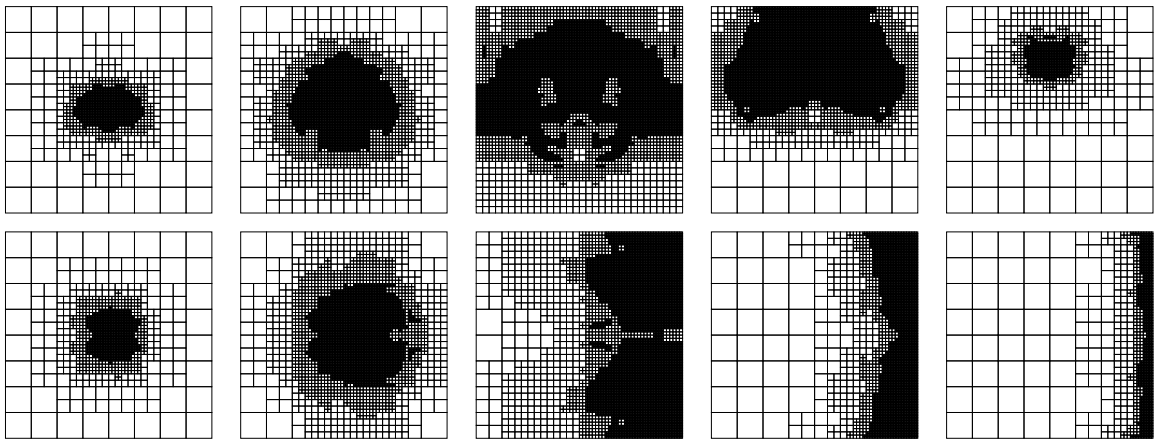

FIG. 2. *Generated grids for the first (top row) and second example (bottom row), at times* $t = 0, 0.3, 0.8, 1.25, 1.75$.

(see [3, 2]). For both examples, we set the initial values to $\mathbf{u}^0(\mathbf{x}) = g(|\mathbf{x}|), \mathbf{v}^0 = 0$, with $g(r) = \frac{1}{2}\cos(10\pi r) - \frac{1}{2}$ for $r < 0.1$ and $g(r) = 0$ otherwise. The numerical solution is sought on the square $(-1, 1)^2$. This configuration and the displacements in x- and y-directions are shown in Fig. 1. Pressure waves traveling to the left and right can clearly be distinguished from shear waves traveling vertically.

Point value As a first example, we consider the mean displacement in x-direction at the point $\mathbf{x}_0 = (0, 0.5)$: $J(\{\boldsymbol{\varphi}, \boldsymbol{\psi}\}) = \int_0^T \varphi_1(\mathbf{x}_0, t)\, dt$, for $T = 1.75$. The end time is chosen such that the shear waves reflected from the top boundary travels over $\mathbf{x}_0$ again. As can be seen from Fig. 2, the grid tracks only that part of the outgoing wave which lies inside the domain of influence of the target functional, which constricts towards $\mathbf{x}_0$ as t approaches T. In [3], it was shown that such grids are not only more efficient than global refinement, but also than grids produced by "traditional" error estimators.

The accuracy of the error estimator is evaluated for a sequence of successively refined grids in the following table. i denotes the refinement step, N the number of degrees of freedom accumulated over time, $J(\mathbf{w}_h)$ the computed value for the target functional, $E = 0.0384 - J(\mathbf{w}_h)$ the "true" error, where 0.0384 is an estimate for the exact value obtained by computations on a very fine grid, and $\sum \eta_K^n$ the estimated error. While the estimated error is not quite in agreement with the actual one, it is within reasonable distance and also correctly predicts the sign.

i	N	$J(\mathbf{w}_h)$	E	$\sum_{n,K} \eta_K^n$
0	126,324	0.03602	$2.4 \cdot 10^{-3}$	$1.2 \cdot 10^{-3}$
1	418,216	0.03762	$7.8 \cdot 10^{-4}$	$2.4 \cdot 10^{-3}$
2	2,676,712	0.03867	$-2.7 \cdot 10^{-4}$	$-4.6 \cdot 10^{-4}$
3	17,265,660	0.03856	$-1.6 \cdot 10^{-4}$	$-3.5 \cdot 10^{-4}$

Boundary displacement As a second example we will consider the mean tangential displacement at the right boundary: $J(\{\boldsymbol{\varphi}, \boldsymbol{\psi}\}) = \int_0^T \int_{-1}^1 \varphi_2(1, y, t)\, dy\, dt$, again with $T = 1.75$. Obviously, again, since the integral extends only to $t = T$, as t approaches

the final time, the domain of influence of $J(\cdot)$ constricts to the right boundary. The effect on the grids can be seen from Fig. 2. Note that the exact solution is the same as for the first example.

In order to evaluate the properties of (6) as an error estimator, we first remark that due to symmetry, the exact value of the target functional is zero. In practice, the value for $J(\mathbf{w}_h)$ will be nonzero due to inexact solution of the discrete equations (for comparison, we note that the stopping criterion for the iterative linear solvers was 10^{-12}). The following table summarizes the numerical value $J(\mathbf{e}) = -J(\mathbf{w}_h)$ and the computed estimates $\sum_{n,K} \eta_K^n$ for a sequence i of successively refined grids with N degrees of freedom accumulated over time:

i	N	$J(\{\mathbf{e}_u, \mathbf{e}_v\})$	$\sum_{n,K} \eta_K^n$	$\sum_{n,K} \lvert\eta_K^n\rvert$
0	41.984	$-4.0 \cdot 10^{-12}$	$-1.9 \cdot 10^{-10}$	1.3
1	155.214	$-9.9 \cdot 10^{-12}$	$-5.8 \cdot 10^{-11}$	2.1
2	952.928	$-2.4 \cdot 10^{-11}$	$-7.1 \cdot 10^{-11}$	2.3

As can be seen, the estimated error is within reasonable distance to the true error, although the latter is only on the same scale as the iteration error.

To compare our error estimate with other approaches, we note that the contributions η_K^n of most space-time cells to the sum are significantly different from zero. However, they mostly cancel out, since if the grid is symmetric about the x-axis for contributions on cells K around $\mathbf{x}_K = (x_K, y_K)$ and K' around $\mathbf{x}_{K'} = (x_K, -y_K)$ there holds: $\eta_K = -\eta_{K'}$. However, most other approaches will not catch this effect since usually at some place in their derivation absolute values are taken; the last column of the table therefore shows the sum of the absolute values of the error indicators, to demonstrate that the error indicators are accurate enough to guarantee cancellation of ten orders of magnitude.

5 Conclusions

A combined approach to error estimation and mesh refinement has been presented. It was shown how to derive the error estimator, using the residuals of the equations and weights obtained from a dual problem, which is solved numerically. We then presented two examples which illustrated the types of grids produced by our approach as well as the quality of the estimated error, which in general is within reasonable bounds of the true error.

References

[1] W. Bangerth, *Adaptive Finite-Elemente-Methoden zur Lösung der Wellengleichung mit Anwendung in der Physik der Sonne*, thesis, University of Heidelberg, 1998.

[2] W. Bangerth and G. Kanschat, *Concepts for object-oriented finite element software – the* ***deal.II*** *library*, Preprint 99-43 (SFB 359), IWR Heidelberg, Oct. 1999.

[3] W. Bangerth and R. Rannacher, *Finite element approximation of the acoustic wave equation: Error control and mesh adaptation*, East–West J. Num. Math., (1999). To appear.

[4] R. Becker and R. Rannacher, *A feed–back approach to error control in finite element methods: Basic analysis and examples*, East–West J. Num. Math., 4 (1996), pp. 237–264.

[5] ——, *Weighted a posteriori error control in FE methods*, in Proceedings of ENUMATH 95, in Proceedings of ENUMATH 97, H. G. Bock et al., eds., Singapore, 1998, World Scientific.

[6] K. Eriksson and C. Johnson, *An adaptive finite element method for linear elliptic problems*, Math. Comp., 50 (1988), pp. 361–383.

[7] C. Johnson, *Discontinuous Galerkin finite element methods for second order hyperbolic problems*, Comput. Methods Appl. Mech. Engrg., 107 (1993), pp. 117–129.